ACS OMEGA

http://pubs.acs.org/journal/acsodf

Article

Influence of Aeration Pipe Length on Oxygen Mass Transfer Efficiency in Terms of Bubble Motion Flow Field

Cheng Lu,* Wen Cheng, Xiaohui Sun, Jiehui Ren, Min Wang, and Tian Wan

Cite This: *ACS Omega* 2022, 7, 39624−39635

Read Online

ACCESS | Metrics & More | Article Recommendations

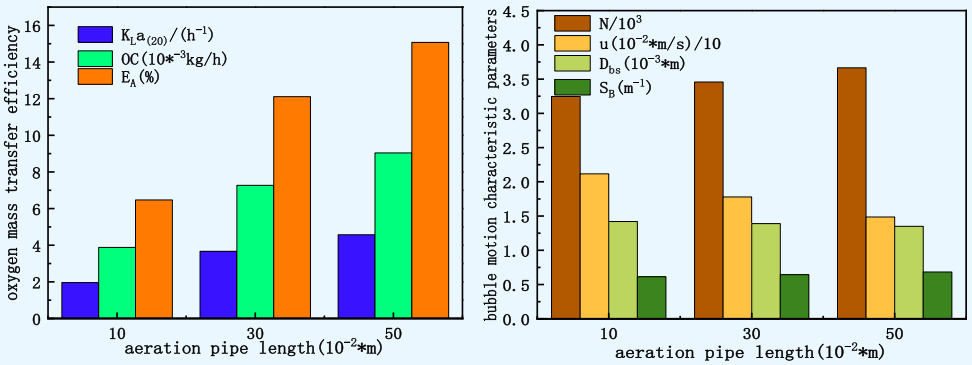

ABSTRACT: Improving the gas−liquid mass transfer efficiency in microporous aeration technology is the key to strengthening the restoration effect of black and odorous water bodies. However, the effect of bubble motion characteristics on oxygen mass transfer has not been systematically studied, which limits the efficient and economical application of microporous aeration remediation technology in black and odorous water. The influence under different aeration pipe lengths was analyzed for oxygen mass transfer and bubble movement in microporous aeration technology. The aeration pipe length (0.1−0.5 m) was positively correlated (R = 1.000, R = 0.997) with the number of bubbles and the specific surface area of bubbles and negatively correlated with the time-average velocity of bubbles and Sauter average diameter (R = −0.999, R = −0.997). Moreover, the increase in pipe length weakened the disturbance intensity of plume to water body. The results of oxygen mass transfer showed that the oxygen mass transfer coefficient (K_La) and oxygen utilization rate (E_A) increased (K_La from 1.96 to 4.57 h^{-1}, E_A from 6.47 to 15.07%) with the increase of pipe length, which was significantly positively correlated (R = 0.985, R = 0.969) with the number of bubbles and bubble specific surface area (S_b). This study provided theoretical parameters for the mechanism of oxygen mass transfer during microporous aeration.

1. INTRODUCTION

Nowadays, the pollution of black and odorous water bodies needs to be treated urgently. Common technologies include sediment dredging, chemical flocculation, bio-ecological restoration, and artificial aeration. Dredging is effective in controlling endogenous pollution,[1−3] but it is liable to cause pollutant release and secondary pollution with large quantity and high cost.[4] Chemical flocculation[5−8] is easy to operate and quickly obtains results but easily destroys the water ecological environment. Bio-ecological restoration can effectively control black and odorous water bodies.[9−11] It has a low cost and stable effect, but it is greatly affected by environmental factors. As the low concentration of dissolved oxygen (DO) is the key factor for the formation of black odor in water bodies, artificial aeration has been widely used. Aeration can increase the concentration of DO; enhance the turbulence of the water body; promote interaction between organic matter, aerobic bacteria, and DO; degrade substances such as nitrogen and phosphorus;[12−15] and is easy to operate without secondary pollution. Microporous aeration is widely used because of its fine air bubbles and high-efficiency oxygen mass transfer.[16] Compared with the aerators commonly used for microporous aeration, the linear microporous aeration system has been well applied by the Tennessee Valley Authority. The bubbles generated by this system have the characteristics of plume diffusion, and the efficiency of oxygen mass transfer in deep water is more than 90%.[17,18] However, when linear microporous aeration is applied to repair black and odorous water in rivers and lakes with a small water depth, the oxygen mass

Received: February 17, 2022
Accepted: October 18, 2022
Published: October 28, 2022

transfer efficiency is inhibited. The utilization rate of oxygen decreases with the decrease in water depth;[19] when the water depth is 2−5 m, the utilization rate of oxygen is generally about 15%, which results in a large waste of aeration energy consumption. Therefore, the low efficiency of oxygen mass transfer and high energy consumption limit the application of linear microporous aeration in the treatment of black and odorous water. Consequently, the oxygen mass transfer mechanism of linear microporous aeration needs to be studied to optimize operating conditions and improve oxygen mass transfer efficiency.

Scholars at home and abroad have conducted extensive research on the mechanism of oxygen mass transfer. Yin, Hu, Zhuang, Stenstrom, and Wei[20−24] studied the effects of aeration volume, aeration density, aeration aperture, water depth, and aeration mode on oxygen mass transfer. Most of these studies were based on macroparameters and lack analyses on the micro-mechanism of oxygen mass transfer. Some scholars also carried out the oxygen mass transfer studies at the microporous level through experimentation or numerical simulation. Although Vélez-Cordero, Liu, McClure, and Deng[25−28] studied the effects of bubble size characteristics and bubble movement speed on oxygen mass transfer, most of these studies were not combined with aeration conditions but only the relationship between bubble movement and oxygen mass transfer mechanism under theoretical conditions. In recent years, some scholars have used particle image velocimetry (PIV) to obtain bubble motion images. They obtained bubble motion characteristics and explored the oxygen mass transfer mechanism based on bubble motion characteristics. Du and Dong[29,30] combined PIV technology with DO monitoring to study the effect of aeration rate on liquid phase flow characteristics and oxygen mass transfer, but the corresponding research still lacked systematic analysis.

The bubble group of linear microporous aeration can be considered as a bubble plume. The movement of bubble plume was random and the structure was relatively complex,[31] which were also studied by some scholars. Cerqueira et al.[32] used PIV laser-induced fluorescence (PIV/LIF) tracer particles to characterize the bubble plume. The results show that the distribution of the turbulence intensity is changed by the axial average velocity and bubble size distribution. Li et al.[33] used PIV to measure the velocity field in the plume and obtained the influence of the plume width, centerline velocity, volume flux, momentum flux, momentum amplification factor, and entrainment coefficient on plume motion. Cheng and Meng[34,35] discussed the effects of aspect ratio, porosity and pressure on plume flow field; Cheng et al.[36] studied the bubble plume in a laboratory-scale three-dimensional bubble column. The influence of different ventilation flow rates, hole spacings, and transverse flow velocities on the stability of the bubble plume is discussed.[37] Most of these studies discussed flow characteristics from the perspective of hydraulics and combined them with gas−liquid oxygen mass transfer to explore the mechanism of oxygen mass transfer.

When linear microporous aeration was applied, some scholars have studied the change rule of oxygen mass transfer efficiency when the pore size of aeration tube changes[38,39] and explored the change mechanism of oxygen mass transfer from the perspective of bubble movement flow field.[39] Nevertheless, the length of the aeration pipe affected the initial size and velocity of bubbles when the aeration volume, aperture, and the volume of repaired water area were certain,[40] thus affecting the shape of bubble plume, gas−liquid mass transfer, and water restoration effect. On the basis of the above investigation and analysis, this paper aimed to obtain the moving image of bubble plume of linear microporous aeration through PIV technology; obtain the gas-phase flow field characteristics such as plume morphological characteristics, time-average vector velocity field, and size characteristics by using PIV post-processing software; monitor the DO concentration; and obtain simultaneously the variation law of oxygen mass transfer efficiency. Combined with the above analysis, this paper systematically studied the influence of bubble plume flow field on oxygen mass transfer under different aeration lengths.

2. MATERIALS AND METHODS

2.1. Experimental Materials and Equipment. The experimental devices are a linear microporous aeration system and a PIV velocity measurement system, which were used to complete the gas−liquid oxygen mass transfer experiment and bubble plume image acquisition.

2.1.1. Linear Microporous Hose Aeration System. The main body of the experimental equipment is a plexiglass box (0.6 m long, 0.45 m wide, and 1 m high). The linear microporous aeration hose is fixed with a stainless-steel pipe (0.01 m in diameter) on one side of the glass box and a tee joint, and the aeration pipe is 0.5 m long (the pipes with lengths of 0.1 and 0.3 m in the experimental conditions are sealed symmetrically along both ends through plastic bags and adhesive tape). The main material of the linear microporous aeration hose is rubber and plastic. A large number of unidirectional pores are found on the hose surface. During aeration, the gas breaks through the pressure and overflows. After aeration is stopped, the pores are closed to prevent the entry of sediment and pollutants. The inner diameter of the hose is 0.009 m, and the outer diameter is 0.011 m. The linear microporous aeration hose is fixed at the bottom of the water body and 0.05 m above the sediment. The height of the horizontal plane of the water tank is 0.9 m. The oil-free air compressor is used to inhale air, which is measured by a gas rotameter. The aeration flow is regulated and controlled by the rotameter, and the inlet pressure is kept constant at 100 kPa through the pressure gauge to avoid fluctuation of the compressor. In this experiment, the aeration system is used to perform the oxygen mass transfer experiment of clean water. A schematic of the device is shown in Figure 1.

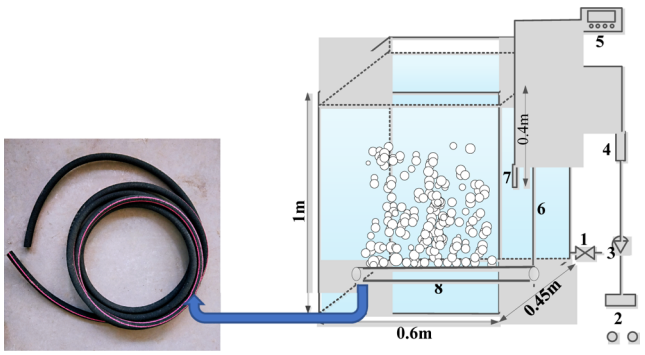

Figure 1. Schematic of microporous hose aeration system. 1—drain valve, 2—air compressor, 3—pressure gauge, 4—gs flowmeter, 5—DO instrument, 6—gas supply pipe, 7—probe, 8—microporous hose aeration.

https://doi.org/10.1021/acsomega.2c00974
ACS Omega 2022, 7, 39624−39635

2.1.2. PIV Velocimetry System. The PIV velocity measurement system used in the experiment comes from Dantec Dynamics A/S in Denmark and is divided into hardware and software. The hardware mainly includes a lighting system, control circuit, and computer system. The software mainly includes image preprocessing (MATLAB), extraction of velocity vector field (TWCPLOT software), and acquisition of bubble size (SHADOW module).[41] The laser model of this PIV instrument is LDY300. The resolution of the high-speed camera, which is produced by LaVision, is 1024 × 1024 pixels. The shooting area is 0.45 × 0.45 m^2 (the water depth on the side of the glass box is 0.40−0.85 m, and the width is 0.45 m). After the area is recorded by the camera, the image is sent to the post-processing system in real time. To ensure the clarity of the image, the light intensity and uniformity of the laser light source were optimized before shooting, and the optimal laser frequency was determined to be 5 S^{-1}. At the beginning of the experiment, the air compressor was opened and the pressure gauge was adjusted according to the reading of the rotor gauge. When the aeration flow was stable, the image was stored at an interval of 0.2 s. Twenty-five images were recorded in each experiment for 5 s. During this time, the bubble can rise by at least 0.45 m. The experimental device of the PIV monitoring system is shown in Figure 2.

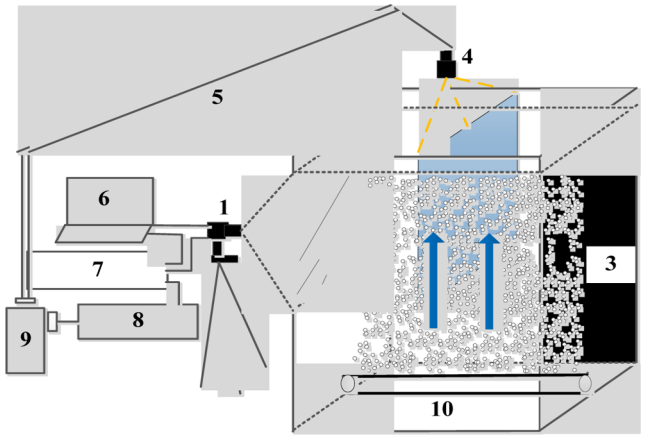

Figure 2. Schematic of the PIV system. 1—high-speed camera, 2—shooting area, 3—shading cloth, 4—chip light source optical element, 5—light arm, 6—computer, 7—synchronous controller, 8—laser controller, 9—pulsed laser, 10—microporous hose aeration.

2.2. Experimental Methods. *2.2.1. Oxygen Mass Transfer Characteristic Experiment.*

(1) The experimental steps of oxygen mass transfer during clear water aeration are as follows:
   (a) Tap water is added into the plexiglass box until the height of the water surface is 0.9 m. Four DO probes are placed 0.2 m below the water surface to monitor the DO concentration and temperature under different working conditions.
   (b))The nitrogen filling method is used to cause oxygen deficiency in the water body, and aeration is performed when the DO concentration drops below 0.5× 10^{-3} kg/m^3 and remains stable. DO and temperature are monitored continuously until DO is saturated. At this point, aeration is stopped and the data are saved.

(2) Calculation principle and method of characteristic parameters of oxygen mass transfer are as follows:

The oxygen mass transfer experiment is mainly based on the classical double-membrane theory proposed by Lewis and Whitman.[42]

1 The total oxygen mass transfer coefficient (K_La) is usually used to characterize the process of gas−liquid mass transfer in water. For theoretical considerations, the Lewis and Whitman's dual-membrane theory was used to describe a log-deficit dependence in eq 1.

$$\ln(C_s - C_t) = \ln C_s - K_L a \times t \quad (1)$$

where C_s (10^{-3} kg/m^3) is the DO saturation concentration, and C_t (10^{-3} kg/m^3) is the DO concentration in the tank at time t (in min).

Water temperature has a great influence on DO concentration. To eliminate the influence of temperature, eq 2 is used to correct the oxygen mass transfer coefficient at different temperatures, which is uniformly converted into the oxygen mass transfer coefficient at 20 °C.

$$k_{La(20\circ C)} = K_{La} \times 1.024^{(20-T)} \quad (2)$$

where $k_{La(20°C)}$—total oxygen mass transfer coefficient at water temperature of 20 °C, h^{-1}; T—actual water temperature, °C.

$$OC = K_{La(20\circ C)} \times V \times (C_S - C_0) \quad (3)$$

where $K_{La(20°C)}$—total oxygen mass transfer coefficient at a water temperature of 20 °C, h^{-1}; V—aeration water volume, m^3; C_S—saturated DO concentration, 10^{-3} kg/m^3. C_0—initial DO concentration, 10^{-3} kg/m^3.

$$E_A = OC \times 100\%/N \times Q \quad (4)$$

where OC—oxygenation capacity (10^{-3} kg/h); N—oxygen content in 1 m^3 atmosphere under standard conditions (kg/m^3), usually 0.28; Q—aeration rate, m^3/h.

(2) Oxygenation capacity (OC [kg/h]) refers to the total concentration of DO transferred to the liquid during gas−liquid mass transfer, which can be calculated by eq 3.

(3) Oxygen utilization [E_A (%)] refers to the percentage of DO used during the gas−liquid mass transfer process in aeration DO concentration. It is calculated by using eq 4.

2.2.2. Image Processing and Flow Field Parameter Acquisition Methods. 2.2.2.1. Image Preprocessing. The original image is processed before analysis to improve the image definition. The spatial gray transformation technology is realized by using MATLAB, which does not change the image pixel position but affects only the gray value of each pixel (Figure 3). The IMHIST function is used to generate the gray histogram of each original image pixel, and the histogram is in the range of 0−255 before adjustment (Figure 3b). However, most pixels are only in the narrow range of 8−28. Most of the corresponding images are dark. In addition, bubbles are almost invisible (Figure 3a). After the contrast is enlarged, the distribution is more uniform (Figure 3d). Finally, bubbles are clearly visible (Figure 3c).

The second correction is based on threshold segmentation technology. The edge is defined as the area with the strongest

https://doi.org/10.1021/acsomega.2c00974
ACS Omega 2022, 7, 39624−39635

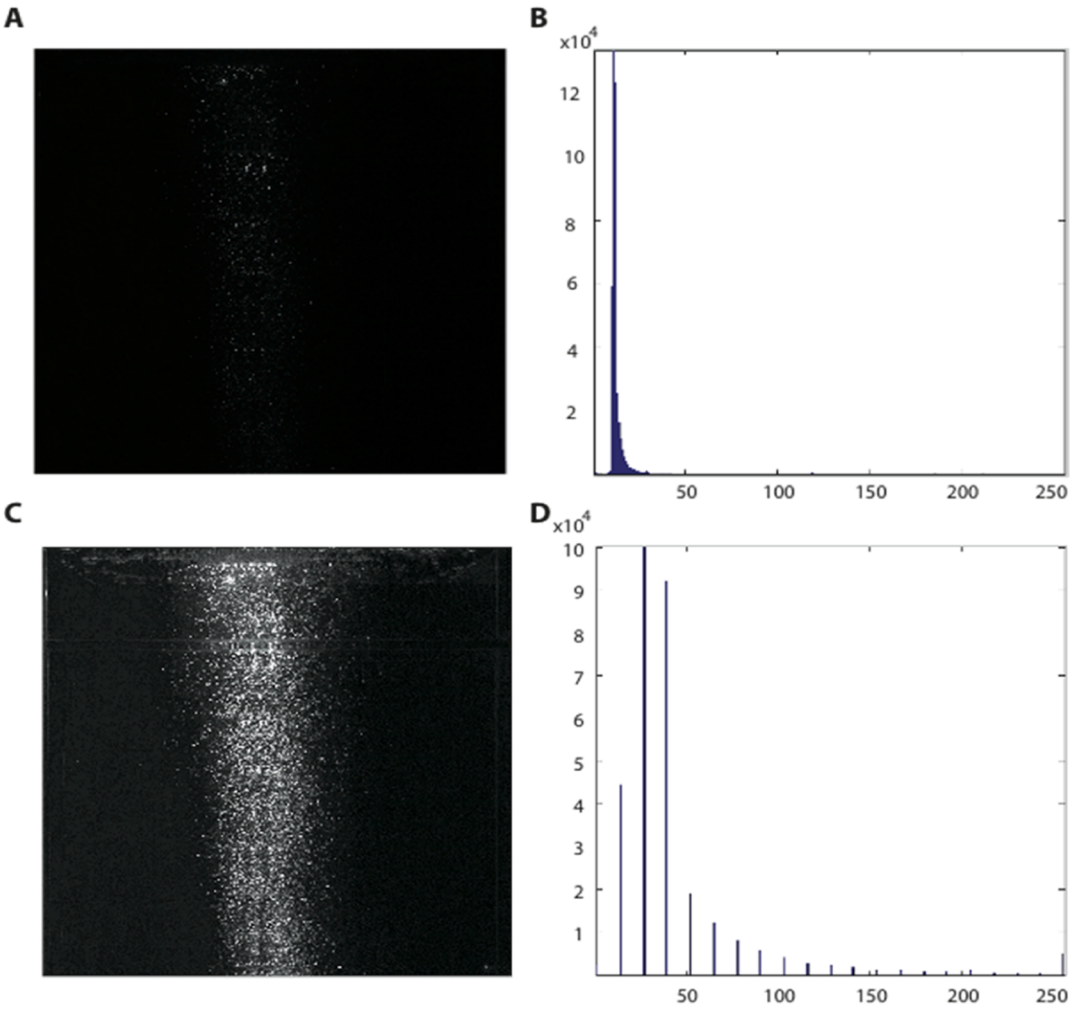

Figure 3. Gray correction of PIV image. Image (a,c) and gray distribution histogram (b,d) before (a,b) and after (c,d) gray correction.

gray change in the image, and PREWITT is used to improve the contrast in Figure 4.

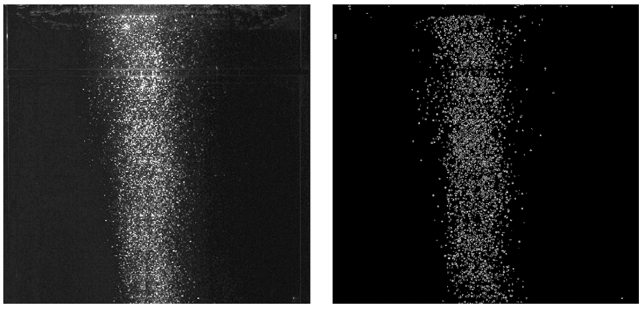

Figure 4. Correction of PIV image edge extraction using PREWITT operator. Images before (left) and after (right) threshold segmentation.

2.2.2.2. Principle and Method of Gas Phase Velocity Field Extraction. The principle of the PIV system acquisition speed is shown in Figure 5. The position of bubbles in the research area is photographed with a high-speed camera. In the dual-frame mode, two frame images of Frame1 and Frame2 are generated. The particle displacement is obtained by using the cross-correlation algorithm, and the instantaneous speed of bubbles is obtained by using the scale derived during

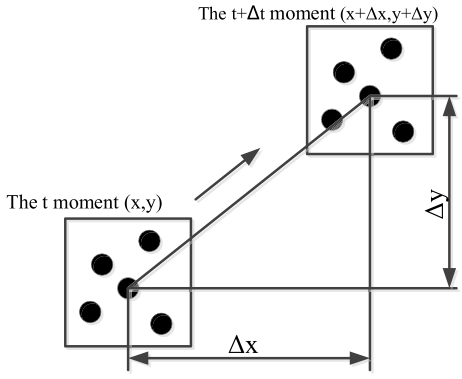

Figure 5. Speed acquisition principle diagram of PIV system.

calibration. Then, the time-average velocity vector field of bubble motion is obtained (eq 5).

The calculation of bubble velocity is based on the comparison of two adjacent frames in two frame modes. After the instantaneous pulse time (as shown in Figure 5), two photos in the mode of two frames are formed, and it also formed displacement difference (ΔX, ΔY) in the two photos. The ratio of the displacement difference (ΔX, ΔY) to the instantaneous pulse time can be regarded as the instantaneous velocity of the bubble. Then, the velocity distribution of the

https://doi.org/10.1021/acsomega.2c00974
ACS Omega 2022, 7, 39624−39635

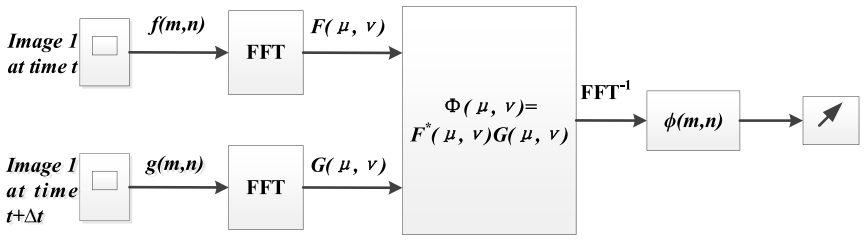

Figure 6. Schematic of the cross-correlation algorithm.

flow field at each time point is obtained from the instantaneous velocity of multiple bubbles at each time point.

The average velocity is obtained by dividing the observed value of bubble displacement in two adjacent frames by the time interval. The signals of two consecutive frames (two time points) must match the same bubble, which can be realized by the cross-correlation algorithm of the adaptive correlation module. The principle is shown in Figure 6. The description for this experiment is as follows: The shooting area of the camera is 0.45 × 0.45 m^2. With the large area of the captured image, each image is segmented into a 64 × 64 grid of query windows to ensure accuracy (one window covers about 0.07 × 0.07 mm^2). Cross-correlation method refers to determining a query window in the first frame image in the dual-frame mode, then finding the window with the closest gray level in the second frame image to match, and performing cross-correlation analysis to speed up.

2.2.2.3. Obtaining Flow Field Parameters.[43] Velocity field acquisition: The displacement of the bubble particles can be obtained by the above cross-correlation algorithm. Thus, the particle velocity can be calculated by eq 5.

$$\begin{cases} u(x, y) = S_X \times k/\Delta t \\ v(x, y) = S_y \times k/\Delta t \end{cases} \tag{5}$$

where S_x, S_y—displacement of particles in the x-direction and y-direction (10^{-3} m); k—scale, the actual length of the pixel per unit scale; dt—time interval between two time points; $u(x,y)$—speed in the x-direction (m/s); $v(x,y)$—speed in the y-direction (m/s); we can extract $u(x,y)$ and $v(x,y)$ through the velocity module of the post-processing software TECPLOT.

Streamline extraction principle: The flow line of bubble movement can reflect the shape, direction, and flow velocity of bubble movement, thus facilitating an analysis of the degree of gas−liquid interaction. In this paper, the streamline module in the PIV system is used to obtain the streamline. The relationship between bubble velocity and stream function is characterized by eqs 6 and 7.

$$u = \frac{\partial \psi}{\partial y}, \qquad v = -\frac{\partial \psi}{\partial y} \tag{6}$$

The stream function can be obtained by integrating the velocity function

$$\psi = \psi_0 + \int -v d_x + u d_y \tag{7}$$

where ψ_0 is the value of stream function at the starting point of integration.

Bubble size feature parameter acquisition: During the rising process, most bubbles have an elliptical shape[44] (Figure 7). The equivalent diameter (d_{bi}) of bubbles is obtained through

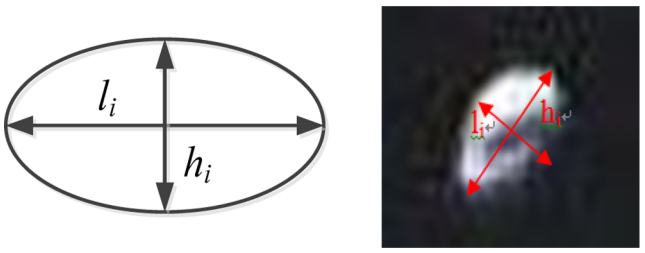

Figure 7. Elliptical bubble diagram.

the corresponding formula, which is equivalent to the diameter of spherical bubbles with the same volume size as the ellipse.

In this paper, the shadow module in the post-processing software TECPLOT of the PIV system is used to obtain the characteristic parameters of the bubble size. As a result of the image preprocessing, the bubbles in the image are clearly visible, thus allowing the number and size of bubbles in the study area to be statistically analyzed.[45] As shown in Figure 7, most of the bubbles in the study area have an elliptical shape, and the upward moving axis is short. We can extract $X_{min}[10^{-3}$ m], $X_{max}[10^{-3}$ m], $Y_{min}[10^{-3}$ m], and $Y_{max}[10^{-3}$ m] of each bubble when using the shadow module to extract the bubble size, and then, we can get the diameter (h_i) of the short axis and its long axis (l_i) ($h_i = Y_{max}[10^{-3}$ m] $- Y_{min}$ $[10^{-3}$m],$l_i = X_{max}[10^{-3}$m] $- X_{min}$ $[10^{-3}$m]). Based on this, we can obtain other bubble size parameters; for example, the equivalent diameter (d_{bi}) is calculated by eq 8. The bubbles can be regarded to have a spherical shape under the condition of the equivalent diameter.[44]

$$d_{bi} = \sqrt[3]{(h_i l_i)^2} \tag{8}$$

The calculation formula of the bubble surface area (S_A) is $S_A = 4\pi(d_{bi}/2)^2$, that of the bubble volume is $V = 4\pi(d_{bi}/2)^3/3$, and that of the bubble specific surface area is $S_b = S_A/V$.

In this experiment, the Sauter average diameter of bubbles is used to represent the average diameter of bubbles, as shown in eq 9.

$$d_{bs} = \sum n_i d_{bi}^3 \Big/ n_i d_{bi}^2 \tag{9}$$

where n_i—number of bubbles with diameter of d_{bi}.

3. RESULTS AND DISCUSSION

3.1. Influence of Aeration Pipe Length on Oxygen Mass Transfer. This part studies the variation characteristics of oxygen mass transfer efficiency under different aeration pipe lengths. The working condition settings are shown in Table 1.

3.1.1. Influence of Dissolved Oxygen Concentration. Under the same aperture (d = 200 × 10^{-6} m) and aeration

https://doi.org/10.1021/acsomega.2c00974
ACS Omega 2022, 7, 39624−39635

Table 1. Experimental Conditions of Oxygen Mass Transfer under Different Aerator Lengths

no.	d (10^{-6}m)	Q (m^3/h)	L (10^{-2}m)
1	200	0.2	10
2	200	0.2	30
3	200	0.2	50

rate (q = 0.2 m^3/h), the variation characteristics of DO concentration in water with time under different aeration pipe lengths are shown in Figure 8. On the basis of the experimental

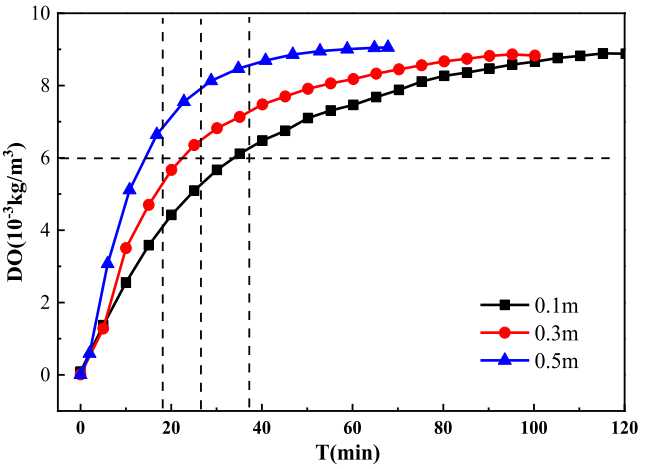

Figure 8. Variation characteristics of DO concentration under different aerator lengths.

steps shown in Section 3.2.1, Figure 1 shows that when the pipe length increased from 0.1 to 0.5 m, the increase rate of DO concentration in the water body increased. When the pipe length increased to 0.5 m, the DO concentration in the water body first saturated, indicating that a long aeration pipe length corresponds to high oxygen mass transfer efficiency when other conditions are the same.

3.1.2. Influence of Oxygen Mass Transfer. The experimental data were analyzed according to the calculation method of characteristic parameters of oxygen mass transfer (Section 2.2.1). The results are shown in Figures 9 and 10. The

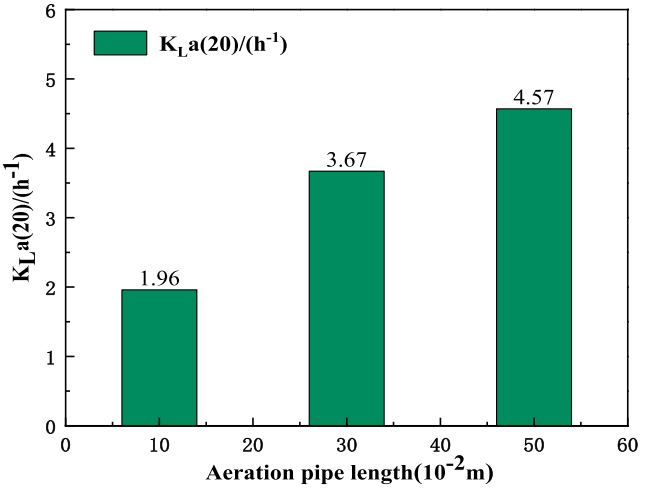

Figure 9. Effect of aeration length on oxygen mass transfer coefficient (K_La).

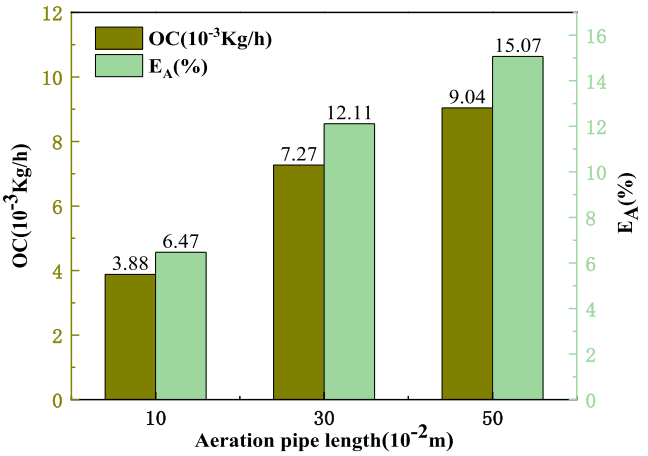

Figure 10. Effect of aeration length on oxygen charging capacity (OC) and oxygen utilization rate (E_A).

influence of aeration pipe length on gas–liquid oxygen mass transfer was analyzed from three characteristic parameters of oxygen mass transfer: oxygen mass transfer coefficient (K_La), oxygenation capacity (OC), and oxygen utilization (E_A). Table 2 explores Pearson's correlation between aeration pipe length and the oxygen mass transfer characteristic parameter.

Table 2. Correlation Analysis of Aeration Pipe Length and Oxygen Mass Transfer Characteristic Parameter

		L	K_La	OC	EA
L	Pearson's correlation	1	0.984	0.984	0.984
	Sig. (double tail)		0.113	0.114	0.113
K_La	Pearson's correlation		1	1.000[a]	1.000[a]
	Sig. (double tail)			0.001	0.000
OC	Pearson's correlation			1	1.000[a]
	Sig. (double tail)				0.001
EA	Pearson's correlation				1
	Sig. (double tail)				

[a]The correlation was significant at the 0.01 level (double tail).

Figures 9 and 10 show that the characteristic parameters of oxygen mass transfer (K_La, OC, and E_A) exhibited an increasing trend (K_La increased from 1.96 to 4.57 h^{-1}, OC increased from 3.88 × 10^{-3} to 9.04 × 10^{-3} kg/h, E_A increased from 6.47 to 15.07%), when the length of the aeration pipe increased from 0.1, 0.3, and 0.5 m. The length of the aeration pipe was positively correlated with oxygen mass transfer parameters (R = 0.984) (Table 2) mainly because different pipe lengths affected the gas holdup, initial bubble size, and initial movement speed. With the increase in the pipe length, the number of outlet holes and the number of bubbles increased, the bubble size decreased,[40] the total gas–liquid contact area increased, and the gas–liquid mass transfer process was strengthened. As the number and size of bubbles increased and decreased, respectively, the gas–liquid contact area per unit volume increased. At the same time, the bubble specific surface area (S_b) increased; therefore, the oxygen utilization rate (E_A) increased. In addition, a long tube corresponds to a small outlet pressure of the bubble. This condition reduced the initial movement speed of the bubble, increased the residence time of the bubble in the water body, provided sufficient time for gas–liquid mass transfer, and strengthened the oxygen mass transfer process efficiency.

https://doi.org/10.1021/acsomega.2c00974
ACS Omega 2022, 7, 39624−39635

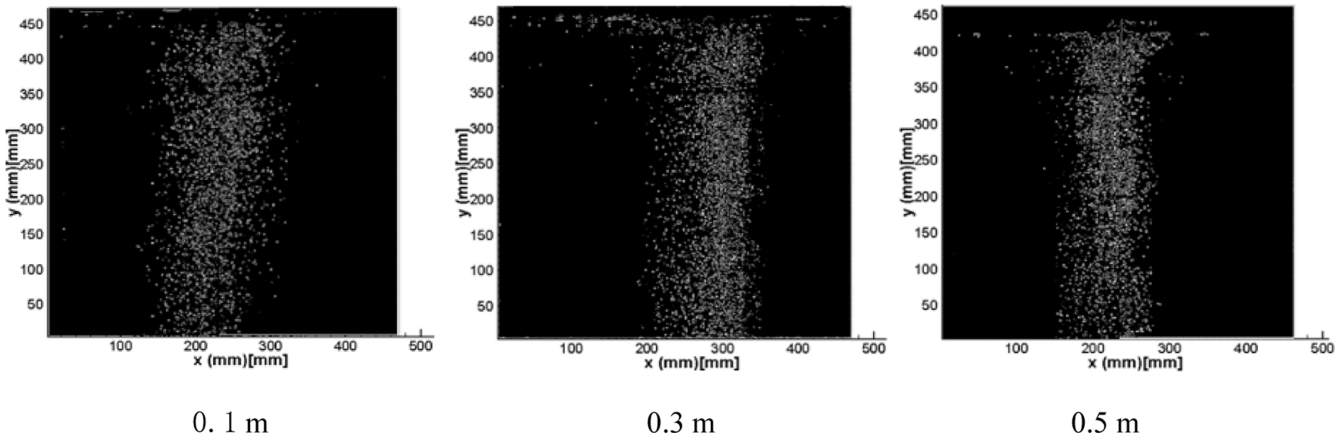

Figure 11. Bubble motion images under each pipe length after gray enhancement and edge segmentation.

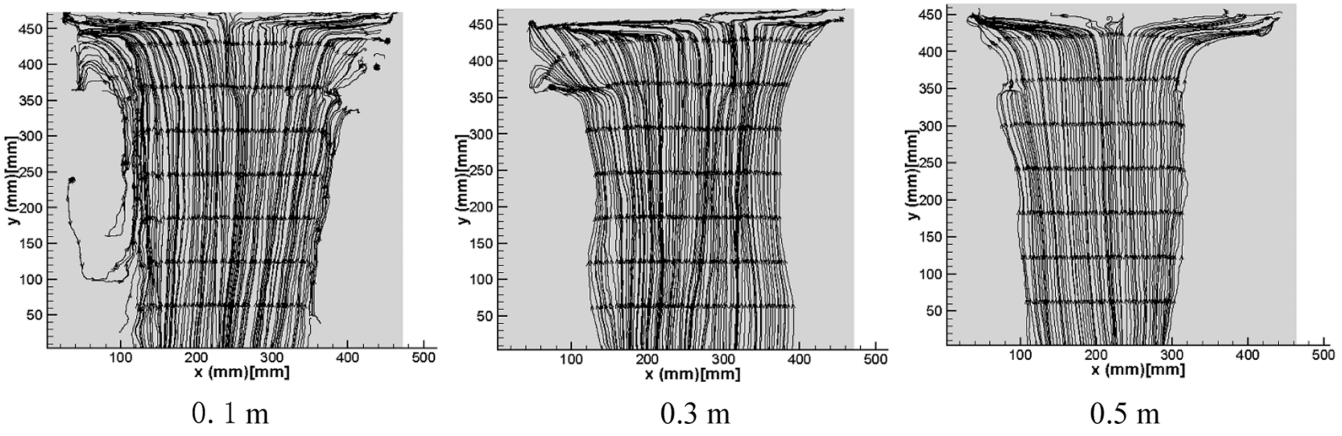

Figure 12. Flow lines of bubble movement under different aeration pipe lengths.

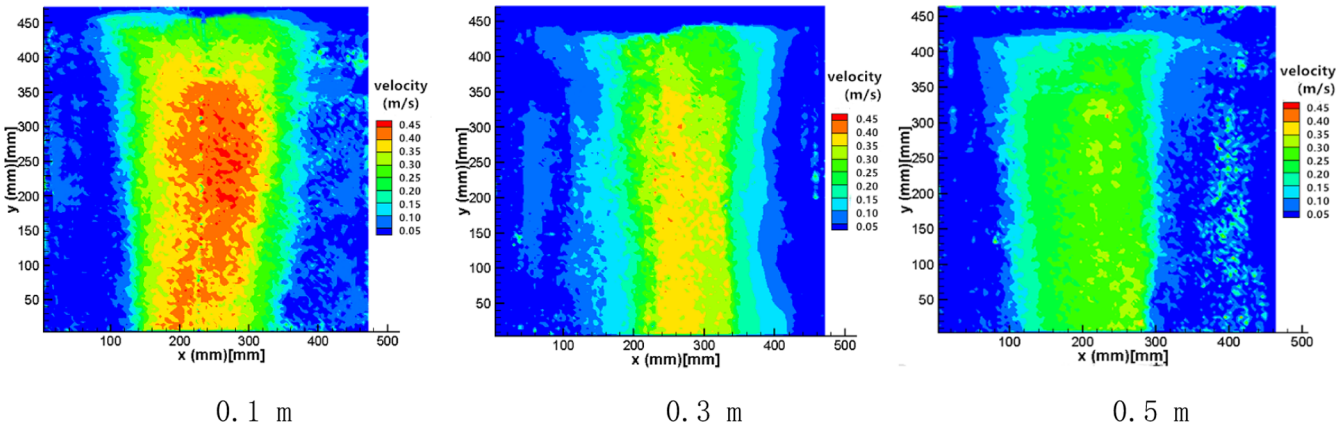

Figure 13. Characteristics of time-average velocity field in the gas phase under different aerator lengths.

Similar trend was observed in the literature,[40,46] where an optimal aeration tube length resulted in the improved oxygen mass transfer coefficient. It is not completely consistent with the conclusion of this study, which may be because the three aeration lengths in this study are distributed on the side of the optimal aeration pipe length. In addition, the purpose of this study is not only to explore the influence of aerated tube length on oxygen mass transfer but more importantly to explore the influence mechanism of the aerated tube length on oxygen mass transfer based on bubble movement characteristics, which would be mentioned in the subsequent analysis.

3.2. Influence of Micropore Pipe Length on Bubble Flow Field Distribution Characteristics. The experimental conditions of bubble plume flow field under different aeration pipe lengths were the same as those in the oxygen mass transfer experiment, as shown in Table 1.

3.2.1. Influence of Aerator Pipe Length on Bubble Plume and Streamline Shape. Figure 11 shows the moving image of a bubble plume processed by gray enhancement and edge segmentation technology in MATLAB. When the tube length increased from 0.1 to 0.5 m, the transverse influence range of bubble plume became smaller. Figure 12 shows the flow line

https://doi.org/10.1021/acsomega.2c00974
ACS Omega 2022, 7, 39624−39635

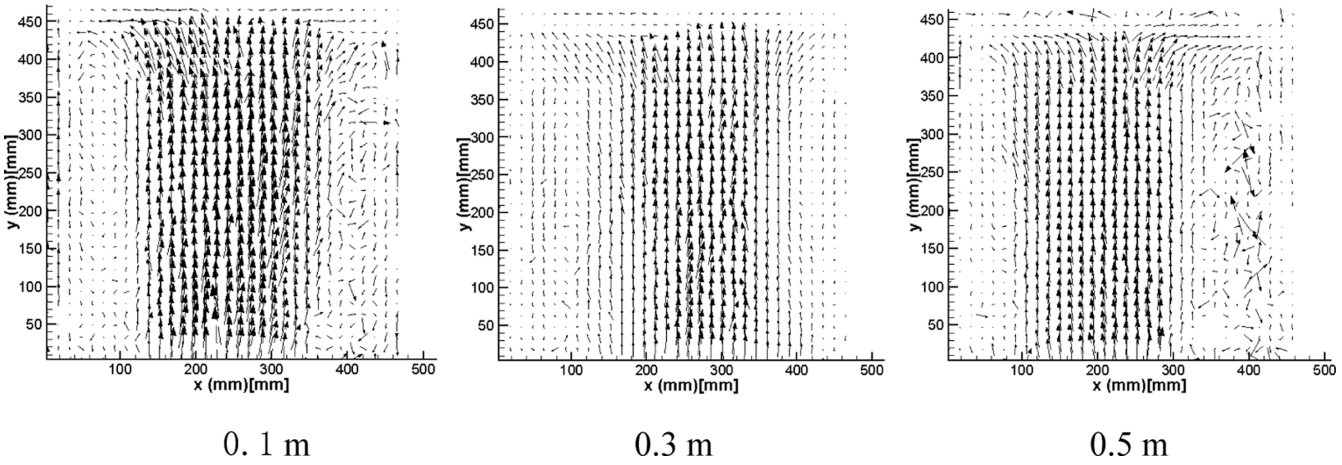

Figure 14. Direction characteristics of mean vector velocity field in the gas phase under different aerator lengths.

extracted by TECPLOT software. At 0.1 m, the bubbles in the lower part of the flow field were relatively concentrated, and the plume had a diffusion trend in the middle and upper parts. This condition was due to the fact that under the same aeration volume, the pipe length was small, the aeration pressure increased, the initial velocity of bubbles increased, the bottom of the transverse diffusion range of the flow line was about 0.2 m, and the middle and upper ranges increased. At 0.3 m, the transverse diffusion range of the plume was about 0.2 m, and no significant difference was found between the transverse influence range of the bottom and the middle and upper parts of the plume, which were caused by the increase in the tube length and the decrease in the bubble outlet pressure. At 0.5 m, the transverse diffusion range of bubble plume was about 0.18 m, the plume shape was more regular, and the bottom was basically the same as the middle and upper parts because of the decrease in the aeration pressure and bubble outlet velocity when the pipe length increased. In short, when the length of the aeration pipe increased from 0.1 to 0.5 m, the shape of the bubble plume gradually became regular and the transverse influence range of plume decreased.

3.2.2. Influence of Aerator Pipe Length on Gas-Phase Velocity Field. Figure 13 shows the time-average velocity nephogram of bubbles under different aeration pipe lengths. At 0.1 m, the time-average velocity of bubbles formed an obvious velocity gradient from the middle to both sides of the plume. Most bubble velocities were concentrated at 0.15−0.35 m/s, some bubbles reached 0.35−0.40 m/s, and the time-average velocity was about 0.212 m/s. At 0.3 m, the time-average velocity also formed an obvious velocity gradient from the middle to both sides of the plume. The velocity of most bubbles was 0.10−0.30 m/s, while that of a few bubbles was about 0.30 m/s, and the time-average velocity was about 0.178 m/s. At 0.5 m, basically no velocity gradient occurred from the middle to both sides of the plume. The bubble velocity was basically 0.10−0.30 m/s, and the time-average velocity was about 0.149 m/s.

Figure 14 shows the gas phase time-average vector velocity field pattern obtained by TECPLOT under different pipe lengths. At 0.1 m, the flow on both sides was significantly affected by the plume, with obvious hydraulic circulation, which increased the intensity of gas−liquid two-phase turbulence. At 0.3 m, the flow on both sides was also affected by the bubble plume, forming a more significant hydraulic circulation, being more obvious on the left side with a larger influence range of the circulation. At 0.5 m, the flow on the left side of the plume was affected by the plume, but to a lesser extent, the flow presented a certain regularity, and the impact of the plume on the flow was significantly weaker than that at 0.1 and 0.3 m.

3.2.3. Influence of Aerator Pipe Length on Bubble Motion Parameters. According to the experimental method in Section 2.2.2, the bubble size characteristic parameters such as bubble number (N), time-average velocity ($U = \sqrt{u^2 + v^2}$), Sauter average diameter (d_{bs}), surface area (S_A), volume (V), and specific surface area (S_b) ($S_b = S_A/V$) under different aeration pipe lengths were calculated by eqs 5−9, as shown in Figures 15 and 16. In Table 3, the correlation between aeration pipe length and bubble size characteristic parameters was discussed by using Pearson's correlation analysis.

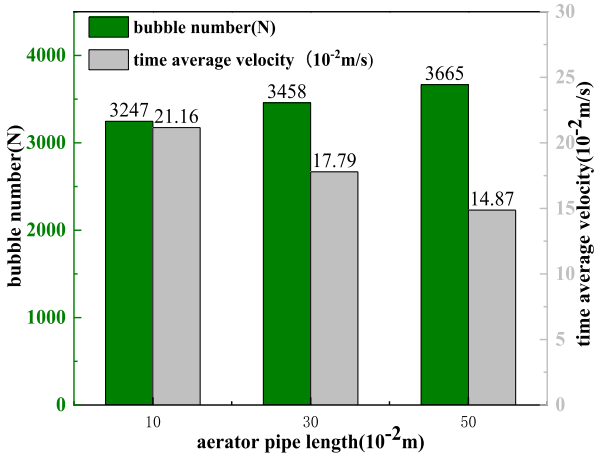

Figure 15. Influence of aerator length on the number of bubbles and average velocity.

As shown in Figure 15, the number of bubbles increased from 3247 at 0.1 m to 3665 at 0.5 m, because when the aeration volume was constant, a long pipe length corresponded to the generation of more aeration holes and bubbles. A positive correlation existed between the tube length and the number of bubbles, and the correlation was significant at the level of 0.01 (double tail) (Table 3). The time-average bubble velocity decreased as the pipe length increased, decreasing from 0.212 m/s at 0.1 m to 0.149 m/s at 0.5 m. When the

https://doi.org/10.1021/acsomega.2c00974
ACS Omega 2022, 7, 39624−39635

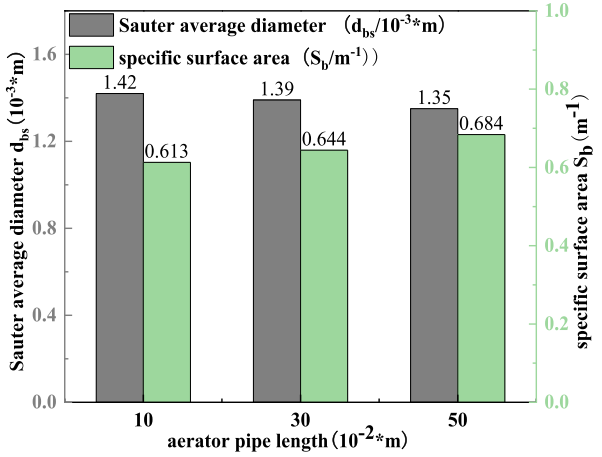

Figure 16. Influence of aerator length on Sauter diameter and specific surface area.

Table 3. Correlation Analysis between Aerator Pipe Length and Bubble Size Characteristic Parameter

		L	N	U	d_{bs}	S_b
L	Pearson's correlation	1	1.000[b]	−0.999[a]	−0.997	0.997[a]
	Sig. (double tail)		0.004	0.026	0.052	0.047
N	Pearson's correlation		1	−0.999[a]	−0.996	0.997
	Sig. (double tail)			0.023	0.056	0.050
U	Pearson's correlation			1	0.992	−0.993
	Sig. (double tail)				0.079	0.073
d_{bs}	Pearson's correlation				1	−1.000[b]
	Sig. (double tail)					0.006
S_b	Pearson's correlation					1
	Sig. (double tail)					

[a]The correlation was significant at the 0.05 level (double tail). [b]The correlation was significant at the 0.01 level (double tail).

aeration volume and aeration aperture remained unchanged, the increase in the pipe length increased the bubble outlet and reduced the bubble outlet pressure and the initial bubble velocity. A negative correlation existed between tube length and bubble velocity (R = −0.999). At the level of 0.05 (double tail), the correlation was significant (Table 3).

Figure 16 shows that the average diameter of bubble Sauter decreased with the increase in the tube length, from 1.42× 10^{-3} m at 0.1 m to 1.35× 10^{-3} m at 0.5 m. The tube length was short, the air outlet holes were fewer, and more opportunities were available for interaction between bubbles in the flow field, thereby increasing the collision and fusion between bubbles as well as the average diameter of bubbles. However, the figure shows that the change in the Sauter average diameter caused by different tube lengths was small. A negative correlation existed between the tube length and the Sauter average diameter of bubbles (R = −0.997) (Table 3). The bubble specific surface area (S_b) increased with the increase in tube length, from 0.613 at 0.1 m to 0.684 at 0.5 m, which was caused by the decrease in the bubble's Sauter average diameter and the increase in the gas−liquid contact area per unit volume. A positive correlation existed between the tube length and bubble specific surface area (S_b) (R = 0.997) at the level of 0.05 (double tail), and the correlation was significant (Table 3).

In Section 3.2, we studied bubble motion characteristics under different aerator lengths, including bubble motion morphological characteristics, mean vector velocity at bubble time, average diameter of bubble, specific surface area of bubble, and so on. There have been many studies on the acquisition of bubble motion characteristics by PIV technology and its post-processing software, but the acquisition of bubble motion characteristics under different aeration lengths is an innovation of this study. Here, we obtained the influence rule of aeration length on each parameter of bubble movement, which is mainly to explore the influence mechanism of bubble movement on oxygen mass transfer at different aeration lengths in combination with the influence rule of aeration length on oxygen mass transfer, which would be discussed in the subsequent analysis.

3.3. Influence of Bubble Motion Characteristics on Oxygen Mass Transfer Efficiency under Different Aerator Lengths. The influence of aeration pipe length on oxygen mass transfer and bubble movement flow field was studied in Sections 2.1 and 2.2 to explore the influence of bubble movement characteristics on oxygen mass transfer efficiency when the pipe length changed.

Figures 9 and 10 show that the oxygen mass transfer efficiency increases as the length of aeration tube increases in this experiment. In addition, the aeration length increases, the time-average velocity decreases, the hydraulic cycle becomes less obvious, and the flow turbulence intensity decreases

Table 4. Pearson's Correlation Analysis of Bubble Motion Characteristic Parameters and Oxygen Mass Transfer Characteristic Parameter under Different Aerator Lengths

		N	U	d_{bs}	S_b	K_La	OC	E_A
N	Pearson's correlation correlation	1	−0.999[a]	−0.996	0.997	0.985	0.985	0.985
	Sig. (double tail)		0.023	0.056	0.050	0.109	0.111	0.110
U	Pearson's correlation		1	0.992	−0.993	−0.991	−0.990	−0.991
	Sig. (double tail)			0.079	0.073	0.087	0.088	0.087
d_{bs}	Pearson's correlation			1	−1.000[b]	−0.966	−0.966	−0.966
	Sig. (double tail)				0.006	0.165	0.167	0.166
S_b	Pearson's correlation				1	0.969	0.968	0.969
	Sig. (double tail)					0.159	0.161	0.160

[a]The correlation was significant at the 0.05 level (double tail). [b]The correlation was significant at the 0.01 level (double tail).

https://doi.org/10.1021/acsomega.2c00974
ACS Omega 2022, 7, 39624−39635

(Figures 12−14). These changes usually weaken oxygen mass transfer. In fact, the oxygen mass transfer efficiency increased in this experiment, as shown in Table 4; that is, the average bubble time velocity was significantly negatively correlated with oxygen mass transfer characteristic parameters (K_La, OC, and E_A) (R = −0.991). This condition is due to many factors that affect oxygen mass transfer. For example, when the bubble velocity decreases, the residence time of bubbles in water increases, which enables more bubbles to complete the gas−liquid mass transfer process and significantly improve oxygen mass transfer efficiency. Thus, the increase in the bubble residence time in water may play a more important role in oxygen mass transfer than the decrease in the bubble average time velocity in this experiment.

The above findings show that a large tube length corresponds to a small Sauter average diameter of the bubble, and a small bubble weakens the water disturbance and the oxygen mass transfer process. Table 4 shows that the average bubble diameter (d_{bs}) was significantly negatively correlated with the characteristic parameters of oxygen mass transfer (R = −0.966). The influence of the Sauter average bubble diameter on the characteristic parameters of oxygen mass transfer was less than that of the number of bubbles. In addition, a small bubble corresponds to a large gas−liquid contact area per unit volume, which is conducive to the increase in oxygen utilization. A significantly positive correlation existed between bubble specific surface area (S_b) and oxygen utilization (E_A) (R = 0.969) (Table 4).

4. CONCLUSIONS

In a linear microporous aeration system, the characteristics of the bubble plume flow field under different aeration pipe lengths and its influence on oxygen mass transfer were investigated synchronously. Combined with the characteristics of the bubble plume flow field, the influence mechanism of oxygen mass transfer was discussed. The following conclusions are drawn:

(1) When the length of the aeration pipe increased from 0.1, 0.3, and 0.5 m, the oxygen mass transfer coefficient (K_La), oxygenation capacity (OC), and oxygen utilization rate (E_A) increased (K_La from 1.96 to 4.57 h^{-1}, OC from 3.88 × 10^{-3} to 9.04× 10^{-3} kg/h, E_A from 6.47 to 15.07%); K_La, OC, and E_A were the largest at 0.5 m.

(2) When the length of the aeration pipe increased from 0.1 to 0.5 m, the shape of the bubble plume gradually became regular and the transverse influence range of plume decreased. The number of bubbles increased from 3247 to 3665, the time-average velocity decreased from 0.212 to 0.149 m/s, the average bubble Sauter diameter decreased from 1.42× 10^{-3} to 1.35× 10^{-3} m, and the bubble specific surface area (S_b) increased from 0.613 m^{-1} at 10 cm to 0.684 m^{-1}. The tube length was positively correlated with the number of bubbles and the specific surface area of bubbles and was negatively correlated with the time-average velocity of bubbles and Sauter average diameter (R = −0.999, R = −0.997). The increase in the pipe length weakened the disturbance intensity of plume to the water body. When the pipe length was 0.1 and 0.3 m, hydraulic circulation was obvious. When the pipe length was 0.5 m, the influence on the flow on both sides was weak.

(3) When the tube length increased, the number of bubbles was significantly positively correlated with K_La and OC (R = 0.985). The increase in bubble residence time in water may play a more important role in oxygen mass transfer than the decrease in bubble time-average velocity in this experiment. The average bubble diameter (d_{bs}) had little effect on oxygen mass transfer. A significantly positive correlation existed between bubble specific surface area (S_b) and oxygen utilization rate (E_A) (R = 0.969).

AUTHOR INFORMATION

Corresponding Author

Cheng Lu − *School of Architecture & Civil Engineering, Xi'an University of Science & Technology, Xi'an 710054, China;* orcid.org/0000-0001-8183-8945; Phone: 15291576536; Email: lucheng.weiyi@163.com

Authors

Wen Cheng − *Institute of Water Resources and Hydro-electric Engineering, Xi'an University of Technology, Xi'an 710048, China*

Xiaohui Sun − *Dezhou Water Conservancy Bureau, Dezhou 253000, China*

Jiehui Ren − *Institute of Water Resources and Hydro-electric Engineering, Xi'an University of Technology, Xi'an 710048, China*

Min Wang − *Institute of Water Resources and Hydro-electric Engineering, Xi'an University of Technology, Xi'an 710048, China*

Tian Wan − *Institute of Water Resources and Hydro-electric Engineering, Xi'an University of Technology, Xi'an 710048, China*

Complete contact information is available at: https://pubs.acs.org/10.1021/acsomega.2c00974

Author Contributions

Data curation, C.L.; formal analysis, C.L. and W.C.; funding acquisition, W.C., M.W., and T.W.; investigation, C.L., X.S., J.R., and T.W.; methodology, C.L., J.R., and T.W.; project administration, W.C., X.S., and M.W.; software, J.R. and T.W.; writing—original draft, C.L.; writing—review and editing, W.C.

Notes

The authors declare no competing financial interest.

ACKNOWLEDGMENTS

C.L., W.C., M.W., and J.R. received funding from the National Natural Science Foundation of China (51809211). T.W. received funding for supplementary experiment from the Shaanxi Water Conservancy Science and Technology Innovation Project (2016slkj-10).

REFERENCES

(1) He, W.; Shang, J. G.; Lu, X.; Fan, C. X. Effects of sludge dredging on the prevention and control of algae-caused black bloom in Taihu Lake, China. *J. Environ. Sci.* **2013**, *25*, 430−440.

(2) Liu, C.; Chen, K. N.; Wang, Z. D.; Fan, C. X.; Gu, X. Z.; Huang, W. Nitrogen exchange across the sediment-water interface after dredging: The influence of contaminated riverine suspended particulate matter. *Environ. Pollut.* **2017**, *229*, 879−886.

(3) Smith, D. R.; Warnemuende, E. A.; Haggard, B. E.; Huang, C. Dredging of drainage ditches increases short-term transport of soluble phosphorus. *J. Environ. Qual.* **2006**, *35*, 611−616.
(4) Cao, C.-J.; Chen, Z. L.; Wang, J.; Huang, M. S.; Qian, C. P.; Lin, L. Review of sediment ecological dredging in urban black-odors river treatment. *J. East China Norm. Univ., Nat. Sci.* **2011**, *2011*, 32−42.
(5) Liao, W. L.; Huang, J. S.; Ding, J. G.; Liu, M.; Chen, T. T.; Tong, Q. B.; Yao, Y.; Lv, S. H. Pollution status and remediation technologies of malodorous black water body in China. *J. Yangtze River Sci. Res. Inst.* **2017**, *34*, 153−158.
(6) Sun, Y. Q.; Yu, I. K. M.; Tsang, D. C. W.; Cao, X. D.; Lin, D. H.; Wang, L. L.; Graham, N. J. D.; Alessi, D. S.; Komárek, M.; Ok, Y. S.; Feng, Y. j.; Li, X. D. Multifunctional iron-biochar composites for the removal of potentially toxic elements, inherent cations, and hetero-chloride from hydraulic fracturing wastewater. *Environ. Int.* **2019**, *124*, 521−532.
(7) Pan, L. T.; Wu, L.; Tu, X. Q. Chemical oxidation-flocculation technology applied for enhanced treatment of polluted river water. *Chin. J. Environ. Eng.* **2007**, *1*, 54−57.
(8) Shuyun, S.; Xiaozhi, G.; Qichao, Z.; Kaining, C. Research on an emergency treatment technology for black-odor water caused by macrophytes decaying. *J. Lake Sci.* **2016**, *28*, 485−493.
(9) Gao, H.; Xie, Y. B.; Hashim, S.; Akhtar Khan, A. A.; Wang, X. L.; Xu, H. Y. Application of microbial technology used in bioremediation of urban polluted river: a case study of Chengnan River, China. *Water* **2018**, *10*, 643.
(10) Li, G. S.; Lei, L. R. Remediation of Black-odorous River with aeration reoxygenation combined with microbial agent porcess. *Environ. Eng.* **2018**, *36*, 34−36.
(11) Pan, M.; Zhao, J.; Zhen, S.; Heng, S.; Wu, J. Effects of the combination of aeration and biofilm technology on transformation of nitrogen in black-odor river. *Water Sci. Technol.* **2016**, *74*, 655−662.
(12) Luo, Q. P.*Effect of Oxygen-Rich Aeration on Migration and Transformation Process of Nitrogen, Phosphorus and Sulfur Iron in Black and Smelly River Chong Qing*; Chong Qing University, 2018.
(13) Guo, N. N.; Qi, Y. K.; Meng, S. L.; Chen, J. C. Glossary research progress on restoration of eutrophic lakes. *Chin. Agric. Sci. Bull.* **2019**, *35*, 72−79. CNKI: SUN: ZNTB. 2019-36-014
(14) Liu, X.; Xie, D.; Li, K. M.; Jin, Z.; Jiang, D. Research on the impact mechanism of different aeration lecel on biogeochemical cycling of nitrogen in sediments. *Ecol. Environ. Sci.* **2011**, *20*, 1713−1719.
(15) Chan, J. Y.; Xu, Z. C.; Luo, Q. J.; Liao, B. H.; Guo, Q. W.; Huang, B. Effect of aeration reoxygenation on sediment transport and transformation of heavy pollution tributaries in Dianchi Lake. *Ecol. Environ.* **2008**, *17*, 2154−2158.
(16) Wang, H. C. Theory and Engineering Practice of microporous aeration System. *Municip. Technol.* **1997**, *1*, 30−37.
(17) Mostefa, M.; Ahmed, A.; Djehiche, D. Study of the oxygen transfer efficiencies in the Different Methods Used in the Technique of Hypolimnetic Aeration. *Adv. Mater. Res.* **2012**, *452*−*453*, 1014−1019.
(18) McGinnis, D. F.; Little, J. C. Predicting diffused-bubble oxygen transfer rate using the discrete-bubble model. *Water Res.* **2002**, *36*, 4627−4635.
(19) Yin, X. F.; Qi, L.; Zhang, X. J.; He, Z. J.; Zhang, Y. K.; Wang, H. C. Research and numerical simulation of the influence of water depth on the oxygenation performance of microporous aeration. *Water Treat. Technol.* **2015**, *41*, 75−78.
(20) Yin, X. F.; Fan, H. T.; Qi, L.; Wang, H. C.; Wei, Y. L.; Jiang, S. Z. Pilot study on the effect of aeration volume and aeration density on aeration performance of microporous aerator. *Environ. Eng.* **2015**, *33*, 27−30.
(21) Hu, P.; Liu, L. H.; Wu, L. X.; Fang, X. X. Study on influencing factors of aeration performance of microporous aeration. *Ind. Water Treat.* **2015**, *35*, 49−52.
(22) Zhuang, J.; Wang, H. C.; Qi, L.; Liu, G. H.; Li, X. D.; Long, H. T. Effect of pore size on aeration performance of micropores. *J. Environ. Eng.* **2014**, *8*, 1723−1726. (in Chinese) CNKI: SUN: HJJZ.0.2014-05-005
(23) Stenstrom, M. K.; Rosso, D.; Melcer, H.; Appleton, R.; Occiano, V.; Langworthy, A.; Wong, P. Oxygen Transfer in a Full-Depth Biological Aerated Filter. *Water Environ. Res.* **2008**, *80*, 663−671.
(24) Wei, Y. L.; Qi, L.; Liu, G. H.; Wang, H. C.; Li, X. D.; Zhuang, J. Influence factors of aeration performance of microporous aerator. *Water Treat. Technol.* **2014**, *40*, 1−7.
(25) Vélez-Cordero, J. R.; Sámano, D.; Yue, P.; Feng, J. J.; Zenit, R. Hydrodynamic interaction between a pair of bubbles ascending in shear-thinning inelastic fluids. *J. Non-Newtonian Fluid* **2011**, *166*, 118−132.
(26) Liu, J. R.; Zhu, C. Y.; Fu, T. T.; Ma, Y. G.; Li, H. Z. Numerical simulation of the interactions between three equal-interval parallel bubbles rising in non-Newtonian fluids. *Chem. Eng. Sci.* **2013**, *93*, 55−66.
(27) McClure, D. D.; Kavanagh, J. M.; Fletcher, D. F.; Barton, G. W. Oxygen transfer in bubble columns at industrially relevant superficial velocities: experimental work and CFD modelling. *CHEM. ENG.* **2015**, *280*, 138−146.
(28) Deng, Z.; Wang, T.; Zhang, N.; Wang, Z. Gas holdup, bubble behavior and mass transfer in a 5m high internal-loop airlift reactor with non-Newtonian fluid. *Chem. Eng.* **2010**, *160*, 729−737.
(29) Du, X. R.; Sun, N.; Wang, M. Study on gas-liquid two-phase flow velocity field under variable aeration based on PIV measurement technology. *J. Hydraul. Eng.* **2015**, *46*, 1371−1377. (in Chinese)
(30) Dong, L.; Zeng, T.; Liu, S. B.; Wang, Y.; Zhang, C. L.; He, Y. Effect of Inlet Flow rate and Aeration intensity on Liquid Flow state and Oxygen Mass Transfer Characteristics in tubular aeration Tank. *Environ. Pollut. Control* **2017**, *33*, 1246−1250.
(31) Cheng, W. J.*Calculation of Void Fraction of Bubble Plume and Its Instability Law*; Xi'an University of Technology: Xi'an, 2010.
(32) Cerqueira, R. F. L.; Paladino, E. E.; Ynumaru, B. K.; Maliska, C. R. Image processing techniques for the measurement of two-phase bubbly pipe flows using particle image and tracking velocimetry (PIV/PTV). *Chem. Eng. Sci.* **2018**, *189*, 1−23.
(33) Li, G.; Wang, B.; Wu, H. J.; DiMarco, S. F. Impact of bubble size on the integral characteristics of bubble plumes in quiescent and unstratified water. *Int. J. Multiphas. Flow* **2020**, *125*, 103230.
(34) Cheng, W.; Wang, M.; Meng, T.*Flow Field Visualization Technology and Its Application in Water Environment*; Science Press: Beijing, 2019; pp 4−5.
(35) Wang, M.*Experimental Study and Numerical Simulation of Two-phase Flow in Gas−Liquid Reactor*; Xi'an University of Technology: Xi'an, 2016.
(36) Cheng, Y. X.; Zhang, Q.; Jiang, P.; Zhang, K. D.; Wei, W. Investigation of Plume Offset Characteristics in Bubble Columns by Euler-Euler Simulation. *Processes* **2020**, *8*, 795.
(37) Cheng, Y. X.; Zhao, N.; Zhang, K. D.; Wei, W. Research on the plume stability of air bubble curtains under low transverse flow velocity environment in dredging engineering. *Ocean Eng.* **2021**, *232*, 109133.
(38) Herrmann-Heber, H. H.; Ristau, R.; Mohseni, M.; Reinecke, F. R.; Hampel, H. Experimental Oxygen Mass Transfer Study of Micro-Perforated Diffusers. *Energies* **2021**, *14*, 7268−7281.
(39) Lu, C.; Cheng, W.; Zhou, S. N.; Wang, M.; Liu, J. K.; Wan, T. Influence of Aeration Microporous Aperture on Oxygen Mass Transfer Efficiency in Terms of Bubble Motion Flow Field. *ACS Omega* **2021**, *6*, 2790−2799.
(40) Li, R.*Optimal Bubble Group Theory of Microporous Aeration and Its Application in Reoxygenation Engineering*; Huazhong University of Science and Technology, 2007.
(41) Wang, T.*Study on Particle Image Velocimetry Technology Based on PIV/PTV Hybrid Algorithm*; Nanjing University of Science and Technology: Nanjing, 2016.
(42) Fick, A. E. V. On liquid diffusion. *Philos. Mag.* **1855**, *10*, 30−39.

https://doi.org/10.1021/acsomega.2c00974
ACS Omega 2022, 7, 39624−39635

(43) Wang, M.*Study on Bubble Plume Movement and Oxygen Transfer Law in Cylindrical Aeration Vessel*; Xi'an University of Technology: Xi'an, 2012.
(44) Xie, Y. N.*Experimental and Numerical Simulation on Aeration performance of Microbubble Diffusion Aeration System*; South China University of Technology: Guangdong, 2018.
(45) Deng, X. W.; Liu, J. T.; Wang, Y. T.; Zhang, C. X.; Xing, B. L. Based on the bottom of the cyclone flotation column inside the bubble size distribution. *J. China Inst. Min.* **2018**, *47*, 1092−1097.
(46) Cheng, X. J.; Zeng, Y. X.; Xie, J.; Gong, W. B. Effect of microporous aeration flow rate and aeration tube length on aeration performance of water body. *Trans. Chin. Soc. Agric. Eng.* **2014**, *30*, 209−217.

https://doi.org/10.1021/acsomega.2c00974
ACS Omega 2022, 7, 39624−39635